Journal of Power Sources 193 (2009) 470–476

Contents lists available at ScienceDirect

Journal of Power Sources

journal homepage: www.elsevier.com/locate/jpowsour

Development of durable carbon black/titanium dioxide supported macrocycle catalysts for oxygen reduction reaction

Xuguang Li [a,*], Changpeng Liu [a], Wei Xing [a], Tianhong Lu [a,b]

[a] Changchun Institute of Applied Chemistry, Chinese Academy of Sciences, Changchun 130022, China
[b] College of Chemistry and Environmental Science, Nanjing Normal University, Nanjing 210097, China

ARTICLE INFO

Article history:
Received 16 February 2009
Received in revised form 27 March 2009
Accepted 9 April 2009
Available online 18 April 2009

Keywords:
FeTPP
TiO_2
Support
Catalyst
Oxygen reduction
Stability

ABSTRACT

Carbon black and titanium dioxide supported iron tetraphenylporphyrin (FeTPP/TiO_2/C) catalysts for oxygen reduction reaction (ORR) were prepared by sol–gel and precipitation methods followed by a heat-treatment at temperatures of 400–1000 °C. The FeTPP/C and TiO_2/C were also studied for comparison. The FeTPP/TiO_2/C pyrolyzed at 700 °C exhibits significantly improved stability while maintaining high activity towards ORR in comparison with the FeTPP/C counterpart. The electrochemical study combined with XRD, XPS, and SEM/EDX analyses revealed that the appropriate dispersion of TiO_2 on the surface of FeTPP/TiO_2/C catalysts, which depending on heat-treatment temperature, plays a crucial role in determining the activity and stability of catalysts.

1. Introduction

Though Pt is the most commonly used electrocatalyst for oxygen reduction reaction (ORR) in the polymer electrolyte membrane fuel cells, it has a prohibitive cost and low abundance for the application. In the past four decades, non-precious metal catalysts have been widely studied as a non-Pt oxygen reduction electrocatalyst [1–23]. The non-precious metal catalysts can be prepared from the pyrolysis of transition metal macrocycles (such as iron and cobalt porphyrin/phthalocyanine) or the precursors of nitrogen, transition metal, and carbon. It is recognized that the simultaneous presence of nitrogen, transition metal, and carbon is crucial to produce the active sites of catalysts for ORR. High-temperature pyrolysis can improve the stability and often also the activity of non-precious metal catalysts. However, the nature of active sites of catalysts is still an open question. One of the most widely accepted hypothesis is the metal-N_4/N_2 moiety bound to carbon support plays an important role for ORR [6–8,15–17]. Another hypothesis is that, transition metal is not part of the active sites, but rather serves to facilitate the incorporation of nitrogen into carbon during pyrolysis to produce nitrogen-doped carbon-based catalysts [23,24]. The graphitic (quaternary) and pyridinic nitrogen sites/or structures over the carbon matrix may act as active sites of catalysts for ORR [15–22].

In comparison with the pure platinum, the non-precious metal catalysts, such as macrocycles are cost-effective and exhibit promising catalytic activity for ORR. Moreover, they are inactive for methanol oxidation reaction and thus demonstrate exceptional methanol tolerance while used as the cathode catalyst in direct methanol fuel cells [25,26]. However, the stability of macrocycle catalysts is still unsatisfactory due to the oxidative destruction of the active sites and the defect sites on carbon structures by hydrogen peroxide produced during the two-electron reduction of oxygen and/or by high electrode potentials, which impedes the successful implementation of macrocycle catalysts in fuel cells [27–32].

It is well known that titanium dioxide (TiO_2) has the capability to decompose hydrogen peroxide [33]. Moreover, it has good chemical and redox stability in the acidic environment and has been widely employed as the supporting material for heterogeneous catalysts [34]. In particular, TiO_2 has been successfully used as a low-cost active semiconductor in the photovoltaic cells, the performance of which can be further enhanced by the modification with organic dyes, such as phthalocyanine macrocycles [35,36].

The aim of this work is to improve the stability of the transition metal macrocycle catalysts for oxygen reduction by using titanium dioxide/carbon black (TiO_2/C) composite as support. It was desired that the decomposition and/or reduction rate of H_2O_2 formed during ORR can be enhanced on macrocycle/TiO_2/C catalysts, and thus the selectivity of four-electron pathway of oxygen reduction to

* Corresponding author. Present address: Department of Chemical Engineering, University of South Carolina, Columbia, SC 29208, USA. Tel.: +1 803 777 7398; fax: +1 803 777 8265.
E-mail address: xuguangl@cec.sc.edu (X. Li).

0378-7753/$ – see front matter © 2009 Elsevier B.V. All rights reserved.
doi:10.1016/j.jpowsour.2009.04.007

water can be increased. Moreover, the stability of porous carbon black is also expected to be improved through the protection of TiO_2. In this work, TiO_2/C was prepared by sol–gel method. TiO_2/C supported iron tetraphenylporphyrin (FeTPP/TiO_2/C) catalysts were prepared by precipitation method followed by a heat-treatment in argon at temperatures of 400–1000 °C. The electrocatalytic activity and stability of the catalysts were examined and compared with FeTPP/C and TiO_2/C counterparts. The physical and chemical characterizations were carried out by XRD, XPS, and SEM/EDX techniques. The effect of TiO_2 on the stability and activity of FeTPP/TiO_2/C catalysts was discussed.

2. Experimental

2.1. Preparation of FeTPP/TiO_2/C

1.05 mL of tetrabutyl titanate was slowly added into 50 mL of anhydrous ethanol under stirring at room temperature to obtain solution A. 0.4 mL of nitric acid was added into a solution mixture of 5 mL of deionized water and 50 mL of anhydrous ethanol to obtain solution B. Then the solution A was slowly dropped into the solution B under stirring to obtain a sol. The sol was mixed with 1.875 g of carbon black and then the mixture was stirred and left for 72 h. The product was dried in vacuum at 80 °C for 6 h to obtain carbon supported TiO_2 (TiO_2/C).

150 mg of FeTPP was dissolved in acetone. 850 mg of TiO_2/C was added to this solution and refluxed at 80 °C for 24 h. Subsequently, the suspension was filtered and the precipitate was rinsed thoroughly with ethanol and deionized water. The residue was dried in vacuum at 80 °C for 6 h and then ground into fine powder. The resulting FeTPP/TiO_2/C powder was subjected to a heat-treatment in a quartz tube furnace at temperatures ranging from 400 to 1000 °C for 1.5 h under argon atmosphere. For convenience, non-heat-treated FeTPP/TiO_2/C and the ones heat-treated at different temperatures were denoted as FeTPP/TiO_2/C-non, FeTPP/TiO_2/C-400, FeTPP/TiO_2/C-700, and FeTPP/TiO_2/C-1000, respectively.

2.2. Electrochemical characterizations

Electrochemical measurements were conducted using EG&G Model 273 potentiostat in a conventional three-electrode glass cell. A rotating disk electrode (RDE) with a glassy carbon (GC) electrode (5 mm diameter) coated with the catalyst ink was used as working electrode. 20 mg of catalyst was blended with 1.6 mL of 5 wt% Nafion solution to form a suspension. 5 μL of the suspension was pipetted onto the surface of GC electrode and then dried at room temperature. Pt wire and Hg/Hg_2Cl_2 were used as counter and reference electrodes, respectively. All the potentials are referred with respect to relative hydrogen electrode (RHE) in the text. 0.5 M H_2SO_4 or 0.3 M H_2O_2 + 0.5 M H_2SO_4 was used as the electrolyte. Argon or oxygen was used for the solution deaeration or saturation, respectively. All measurements were carried out at room temperature. The oxygen reduction current was taken as the difference between currents measured in the argon and oxygen saturated electrolytes at a scan rate of 10 mV s^{-1} and electrode rotation rate of 1000 rpm.

2.3. Physical and chemical characterizations

Powder X-ray diffraction (XRD) patterns of the catalysts were obtained with a powder diffraction system (Rigaku D/Max 2500 V/PC) using a Cu Kα source operated at 40 keV at a scan rate of 4° min^{-1}. X-ray photoelectron spectroscopy (XPS, VG ESCA Lab MK II) was performed to analyze the surface concentrations of Fe, N, and Ti on the catalysts. Scanning electron microscopy (SEM, Hitachi S-520) coupled with energy dispersive X-ray analysis (EDX) was

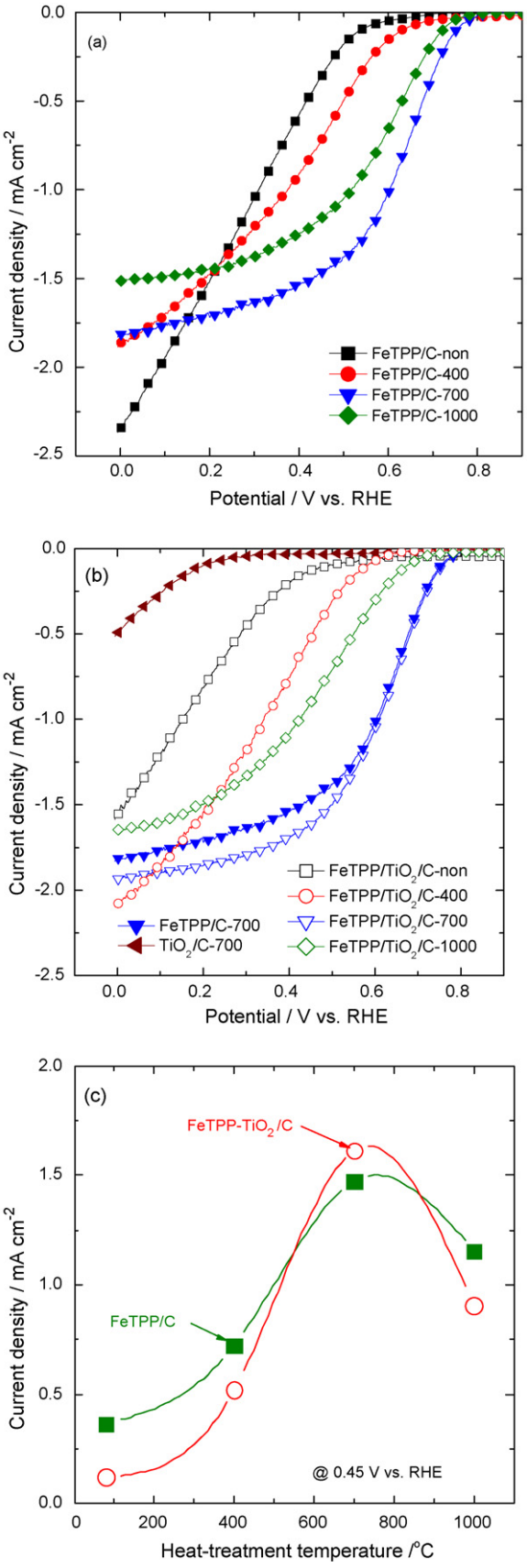

Fig. 1. Polarization curves for oxygen reduction on (a) FeTPP/C and (b) FeTPP/TiO_2/C heat-treated at different temperatures in O_2-saturated 0.5 M H_2SO_4; scan rate, 10 mV s^{-1}; rotation rate, 1000 rpm. (c) Current density of oxygen reduction on FeTPP/C and FeTPP/TiO_2/C at 0.45 V as a function of heat-treatment temperature.

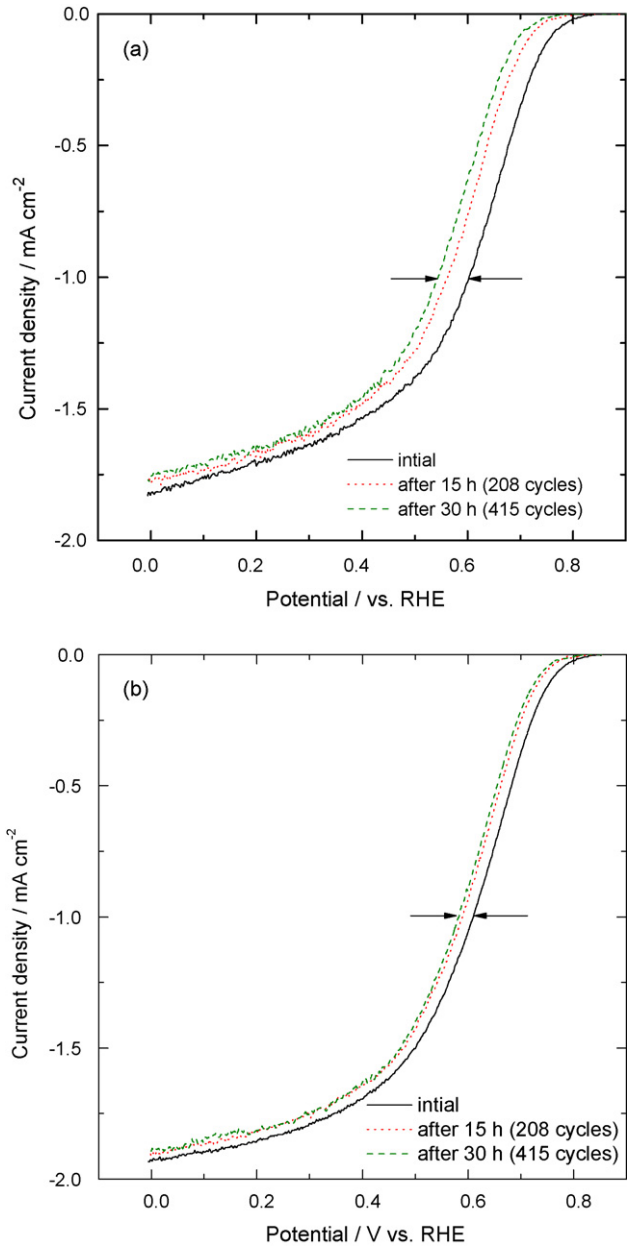

Fig. 2. Polarization curves for oxygen reduction on (a) FeTPP/C-700 and (b) FeTPP/TiO_2/C-700 before cycling test, and after 15 and 30 h cycling test in O_2-saturated 0.5 M H_2SO_4; scan rate, 10 mV s^{-1}; rotation rate, 1000 rpm.

carried out to observe the distribution of Ti near the surface of catalysts.

3. Results and discussion

3.1. Electrocatalytic properties of FeTPP/TiO_2/C

Fig. 1a shows the polarization curves for oxygen reduction on FeTPP/C heat-treated at different temperatures. It is obvious that heat-treatment greatly enhance the catalytic activity of FeTPP/C for oxygen reduction. The pyrolysis at 700 °C gives rise to the best performance of catalyst in terms of the activation overpotential and current density of oxygen reduction. The variation of the current density with potential on the samples heat-treated at 700 and 1000 °C is attributed to the decreased amount of active sites of catalysts with increasing pyrolyzing temperatures. These results

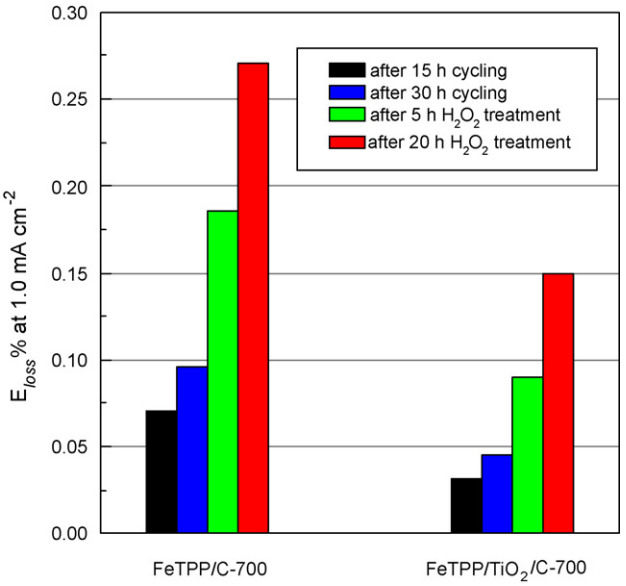

Fig. 3. Percentage of potential loss (E_{loss}%) at 1 mA cm^{-2} for FeTPP/C-700 and FeTPP/TiO_2/C-700 before and after 5 and 20 h exposure to Ar-saturated 0.3 M H_2O_2 + 0.5 M H_2SO_4 solution. For comparison, the corresponding data for FeTPP/C-700 and FeTPP/TiO_2/C-700 before cycling test, and after 15 and 30 h cycling test obtained from Fig. 2 were also presented.

are in accordance with those previously reported in the literatures [7,8,26].

Fig. 1b shows the polarization curves for oxygen reduction on FeTPP/TiO_2/C heat-treated at different temperatures. For comparison, the results on FeTPP/C-700 and TiO_2/C-700 were also presented here. It can be seen that, at high potential, TiO_2/C-700 has no catalytic activity for ORR. The FeTPP/TiO_2/C catalysts behave similarly with FeTPP/C when increasing heat-treatment temperature. The FeTPP/TiO_2/C-700 exhibits comparable activity with FeTPP/C-700.

For clarity, Fig. 1c presents the plots of the current densities of oxygen reduction on FeTPP/C and FeTPP/TiO_2/C at 0.45 V as a function of heat-treatment temperature. The same profiles were observed for both FeTPP/C and FeTPP/TiO_2/C catalysts, sug-

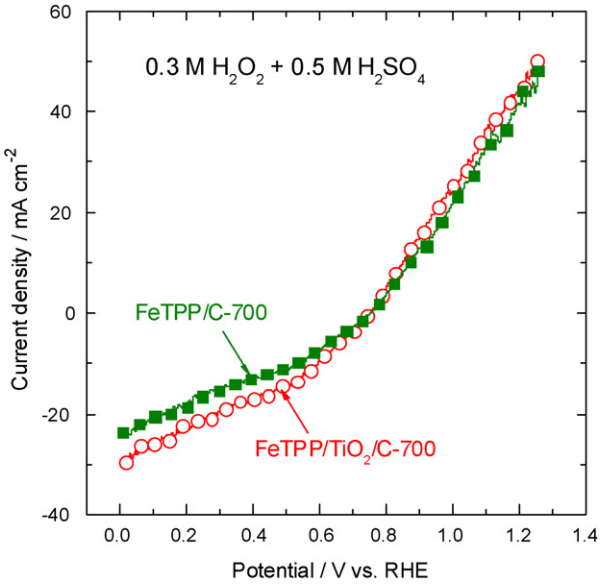

Fig. 4. Polarization curves for H_2O_2 reduction and oxidation on FeTPP/TiO_2/C-700 and FeTPP/C-700 in Ar-saturated 0.3 M H_2O_2 + 0.5 M H_2SO_4; scan rate, 10 mV s^{-1}, rotation rate: 1000 rpm.

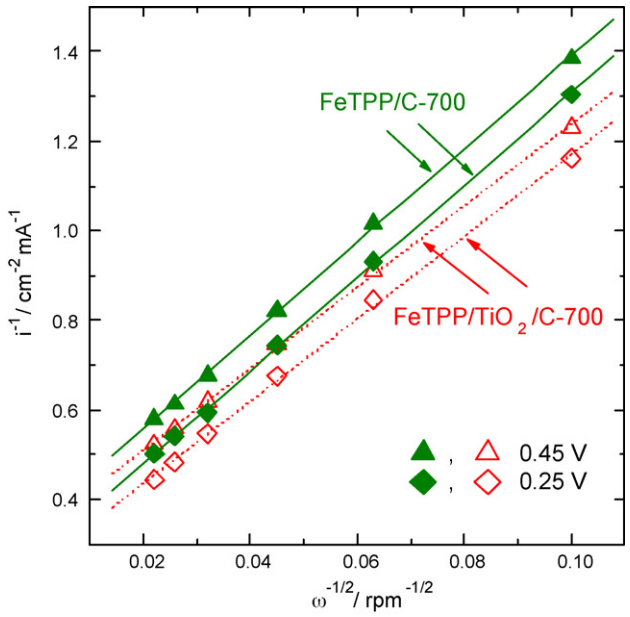

Fig. 5. Koutecky–Levich plots for oxygen reduction on FeTPP/C-700 and FeTPP/TiO_2/C-700 at various potentials.

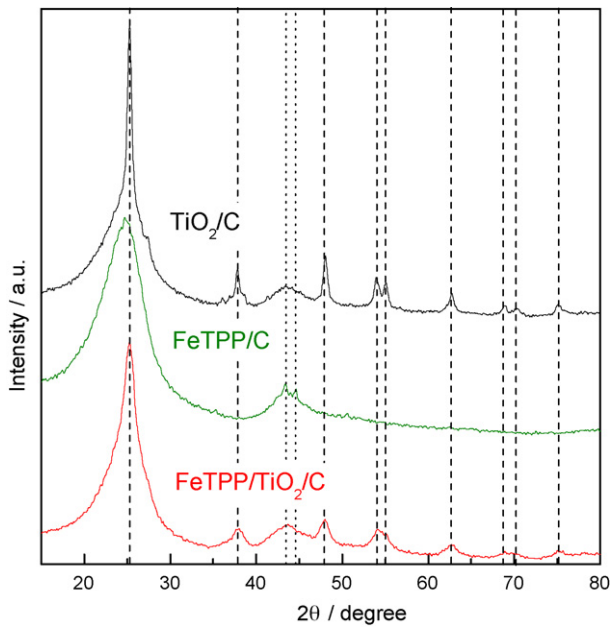

Fig. 7. XRD patterns of FeTPP/C, TiO_2/C and FeTPP/TiO_2/C heat-treated at 700 °C.

gesting that they have similar main catalytic sites. According to the literatures, for the non-precious metal catalysts pyrolized at temperatures lower than 800 °C, the active sites may be the combination of metal-N_4/N_2 structure and nitrogen-modified carbon structure, such as graphitic (quaternary) and pyridinic nitrogen. At heat-treatment temperatures of 800–1000 °C, the active sites of catalysts may be the pyridinic and graphitic (quaternary) nitrogen on the carbon matrix since metal-N_4/N_2 structure decomposes. At above 1000 °C, the active sites may be mainly the graphitic (quaternary) nitrogen [6–24]. Moreover, FeTPP/C shows higher catalytic performance than FeTPP/TiO_2/C except at 700 °C. The possible reason is that the active sites of macrocycle catalysts depositing on TiO_2 cannot work efficiently since TiO_2 as semiconductor has much lower electron conductivity in comparison with carbon black. However, the FeTPP/TiO_2/C heat-treated at 700 °C maintains comparable catalytic activity with FeTPP/C for oxygen reduction. Hence, further study will be focused on the FeTPP/TiO_2/C-700 composite catalyst.

In this work, the stability of catalysts was evaluated by accelerated cycling test protocol. That is, the electrodes are cycled from 0 to 1.3 V vs. RHE in O_2-saturated 0.5 M H_2SO_4 solution with scan rate of 10 mV s^{-1} and electrode rotation rate of 1000 rpm. Fig. 2 shows the polarization curves for oxygen reduction on FeTPP/C-700 and FeTPP/TiO_2/C-700 recorded before cycling test, and after 15 and 30 h cycling test, respectively. It is evident that FeTPP/TiO_2/C-700 shows much higher durability than FeTPP/C-700. At 1 mA cm^{-2}, after 15 h cycling, a negative potential shift with 35 mV was observed for FeTPP/C-700, which is about 67% higher than that for FeTPP/TiO_2/C-700. After 30 h cycling, the performance

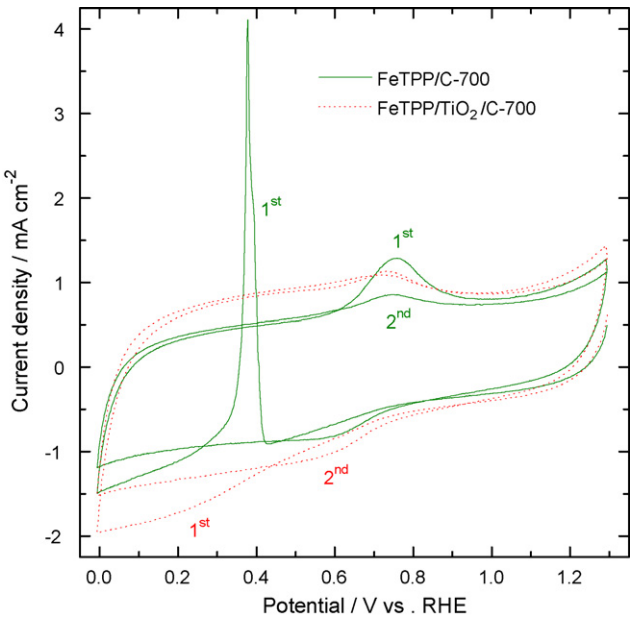

Fig. 6. Cyclic voltammograms of FeTPP/C-700 and FeTPP/TiO_2/C-700 in Ar-saturated 0.5 M H_2SO_4; scan rate, 100 mV s^{-1}.

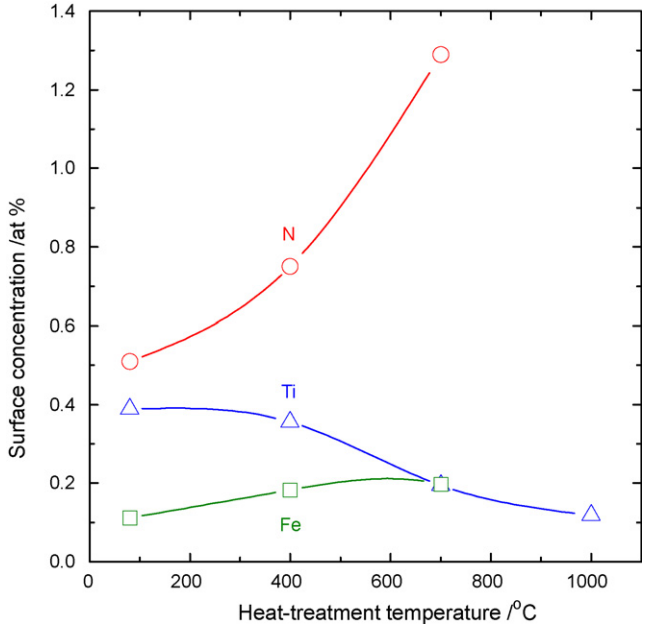

Fig. 8. Surface concentrations of Fe, N, and Ti on FeTPP/TiO_2/C as a function of heat-treatment temperature.

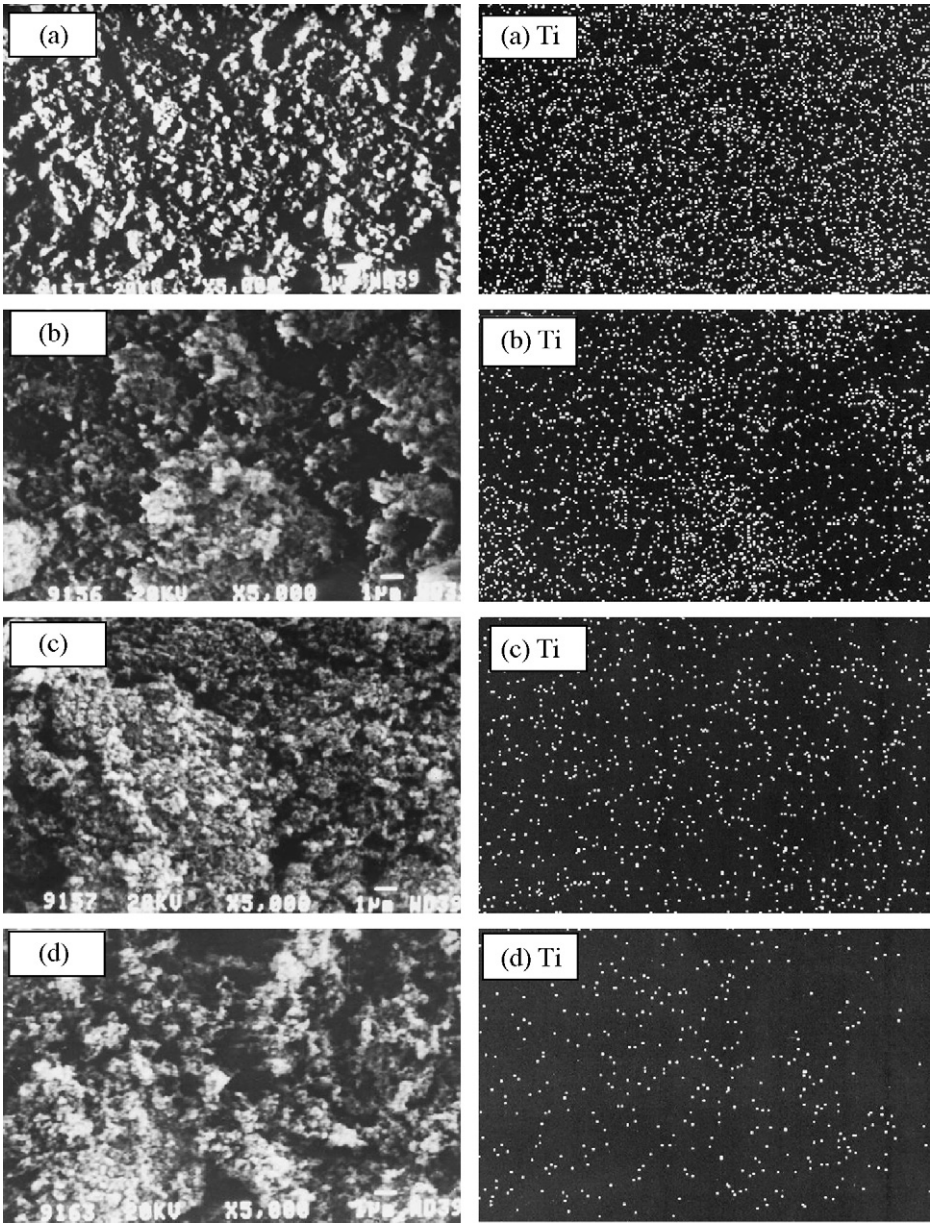

Fig. 9. SEM images (*left*) and distribution maps of the element Ti (*right*) of FeTPP/TiO_2/C heat-treated at different temperatures: (a) FeTPP/TiO_2/C-non, (b) FeTPP/TiO_2/C-400, (c) FeTPP/TiO_2/C-700 and (d) FeTPP/TiO_2/C-1000.

degradation of FeTPP/C-700 is about 200% of that of FeTPP/TiO_2/C-700. This indicated that the application of carbon/TiO_2 composite as the support of macrocylces effectively improves the stability of catalysts when pyrolyzed at 700 °C.

In order to elucidate the origin of the improved stability of FeTPP/TiO_2/C-700 than FeTPP/C-700 counterpart, the effect of H_2O_2 on the activity degradation of catalysts was examined. Fig. 3 shows the percentage of potential loss (E_{loss}%) at 1 mA cm^{-2} for FeTPP/C-700 and FeTPP/TiO_2/C-700 before and after 5 and 20 h exposure to Ar-saturated 0.3 M H_2O_2 + 0.5 M H_2SO_4. For comparison, the corresponding data for catalysts before cycling test, and after 15 and 30 h cycling tests obtained from Fig. 2 were also presented.

The percentage of potential loss, E_{loss}% at 1 mA cm^{-2} is expressed as

$$E_{loss}\% = \frac{E_{ini} - E}{E_{ini}} \times 100\% \quad (1)$$

E_{ini} is initial potential before the exposure to H_2O_2 solution and E is measured potential after the exposure to H_2O_2 solution for a period of time. It is evident that after the exposure to 0.3 M H_2O_2 + 0.5 M H_2SO_4, the catalytic performance decrease of FeTPP/TiO_2/C-700 is much smaller than that of FeTPP/C-700. This tendency is consistent with that of the cycling test. However, it can be seen that the effect of 0.3 M H_2O_2 is much more severe than the cycling test probably due to that the concentration of H_2O_2 used in this work is high. Lefèvre et al also observed that H_2O_2 treatment can lower the catalytic activity of non-precious metal catalysts [29]. These results indicated that FeTPP/TiO_2/C-700 is more resistant to the oxidative attack of H_2O_2 than FeTPP/C-700. Moreover, it can be seen that, the activity degradation of catalysts mainly occurs in the first several hours in both H_2O_2 exposure and cycling test cases.

Furthermore, the catalytic activity of FeTPP/TiO_2/C-700 and FeTPP/C-700 for H_2O_2 reduction was investigated. Fig. 4 shows the polarization curves of H_2O_2 reduction and oxidation on the catalysts in Ar-saturated 0.3 M H_2O_2 + 0.5 M H_2SO_4. It can be seen

that FeTPP/TiO_2/C-700 exhibits higher catalytic activity for the reduction of H_2O_2 than FeTPP/C-700. Therefore, the H_2O_2 produced during ORR can be more efficiently reduced to H_2O on FeTPP/TiO_2/C-700 than on FeTPP/C-700. The high current density observed for the reduction of H_2O_2 is attributed to the high concentration of H_2O_2 used in this experiment [30].

Fig. 5 shows the Koutecky–Levich plots for oxygen reduction on FeTPP/C-700 and FeTPP/TiO_2/C-700. The slope of the plots allows us to check the consistency with the theoretical values according to the equation [36–40].

$$\frac{1}{i} = \frac{1}{i_k} + \frac{1}{i_l} + \frac{1}{i_f} \quad (2)$$

$$i_l = B\omega^{1/2} = 0.62nFD_{O_2}^{2/3}\nu^{-1/6}C_{O_2}\omega^{1/2} \quad (3)$$

$$i_f = \frac{nFC_fD_f}{L} \quad (4)$$

where i is measured current density, i_k, kinetic current density, i_l, diffusion limited current density, i_f, Nafion film diffusion limited current density, B, Levich slope, n, the number of electron exchanged in ORR, F, Faraday constant, C_{O_2}, bulk concentration of oxygen (1.3×10^{-6} mol cm^{-3}), D_{O_2}, diffusion coefficient of oxygen in the bulk solution (1.7×10^{-5} cm^2 s^{-1}), ω, rotation rate in rpm, ν, kinematic viscosity of the solution (0.01 cm^2 s^{-1}), L, Nafion film thickness, C_f, reactant concentration in the Nafion film, and D_f is diffusion coefficient of oxygen in the Nafion film. Since the Nafion film thickness was reduced to the extent that i_f becomes significantly larger than i_k and i_l, the influence of i_f on the measured current density in our experiments was negligible. The experimental B values for FeTPP/C-700 and FeTPP/TiO_2/C-700 are 8.7×10^{-2} and 11.1×10^{-2} mA cm^{-2} rpm$^{-0.5}$, respectively. The theoretical calculated B value for a four-electron ($n = 4$) process is 13.9×10^{-2} mA cm^{-2} rpm$^{-0.5}$. As a result, the calculated n values for FeTPP/C-700 and FeTPP/TiO_2/C-700 are 2.5 and 3.2, respectively. This indicated that FeTPP/TiO_2/C-700 catalyze ORR via four-electron pathway more than FeTPP/C-700. The amount of H_2O_2 formed on FeTPP/TiO_2/C-700 is lower in comparison with FeTPP/C-700.

Fig. 6 shows the cyclic voltammograms of FeTPP/C-700 and FeTPP/TiO_2/C-700 in Ar-saturated 0.5 M H_2SO_4. For FeTPP/C-700, a pair of peaks at 0.6–0.8 V is attributed to the quinone/hydroquinone couple [41–43]. An anodic peak appears at about 0.38 V during the first cycle in the cathodic direction and disappears in the second cycle, which is ascribed to the dissolution of remaining trace amount of metallic Fe on the surface of FeTPP/C-700. For FeTPP/TiO_2/C-700, the anodic peak related to metallic Fe was not observed, suggesting the possible interaction between Fe residue and TiO_2. According to the literatures [6–24] and our experiment, the metallic Fe is not the active site for oxygen reduction.

3.2. Physical and chemical properties of FeTPP/TiO_2/C

Fig. 7 shows the XRD patterns of FeTPP/C, TiO_2/C and FeTPP/TiO_2/C heat-treated at 700 °C. For FeTPP/C-700, the diffraction peaks at 2θ of about 43.4 and 44.6° are attributed to the metallic γ-Fe and α-Fe [7]. Regarding TiO_2/C-700, the characteristic diffraction peaks of TiO_2 were clearly observed [44,45]. In the case of FeTPP/TiO_2/C-700, the metallic Fe diffraction peaks were not observed, which is in good agreement with the cyclic voltammogram results shown in Fig. 6. Moreover, the peaks related to TiO_2 become broader and lower. These may be attributed to the interaction of Fe/N moiety and TiO_2, and/or carbon and TiO_2 [45] when heat-treated at 700 °C. The diffraction peaks of carbon and TiO_2 overlap at 2θ of approximately 25°.

The surface concentrations of Fe, N, and Ti were analyzed by XPS since these elements may be the components of the active sites of catalysts. Fig. 8 shows the surface concentrations of Fe, N, and Ti on FeTPP/TiO_2/C as a function of heat-treatment temperature. The Fe and N concentrations increase with increasing heat-treatment temperature up to 700 °C. At 1000 °C, Fe and N are not detected by XPS. This trend is roughly same with that of catalytic performance of FeTPP/TiO_2/C catalysts for ORR (see Fig. 1b and c). This indicated that the structures containing Fe and/or N may be the active site of FeTPP/TiO_2/C catalysts, which is same with that of FeTPP/C counterpart [6–24]. On the other hand, the Ti surface concentration on the catalysts decreases with the increase of heat-treatment temperature. This result was further confirmed by the distribution maps of element Ti in FeTPP/TiO_2/C catalysts measured by SEM/EDX (Fig. 9). The lower Ti concentration and appropriate Ti dispersion in FeTPP/TiO_2/C-700 catalyst minimizes the adverse effect of low-conductivity TiO_2 between Fe/N based active sites and carbon support. Moreover, the TiO_2 in FeTPP/TiO_2/C-700 may protect carbon from oxidation/corrosion during electrochemical cycling/H_2O_2 attacking through covering the defect sites on carbon structure where carbon oxidation initiates [32].

4. Conclusions

FeTPP/TiO_2/C was prepared by depositing FeTPP on the pre-synthesized TiO_2/C support. The resulting FeTPP/TiO_2/C was heat-treated at temperatures ranging from 400 to 1000 °C. FeTPP/TiO_2/C heat-treated at 700 °C exhibits the improved stability while maintaining a comparable activity to FeTPP/C counterpart for oxygen reduction. This may be partially attributed to the increased selectivity of FeTPP/TiO_2/C catalysts towards ORR by suppressing the formation of H_2O_2 and the enhanced resistivity of FeTPP/TiO_2/C to the oxidative attack of H_2O_2. It was revealed that the appropriate concentration and dispersion of TiO_2 over FeTPP/TiO_2/C catalysts, which depending on the heat-treatment temperatures, play a crucial role in determining the durability and activity of catalysts.

References

[1] R. Jasinski, Nature 201 (1964) 1212–1213.
[2] H. Jahnke, M. Schönborn, G. Zimmermann, Top. Curr. Chem. 61 (1976) 133–181.
[3] J.A.R. van Veen, J.F. van Baar, C.J. Kroese, J.G.F. Coolegem, N. de Wit, H. Colijn, Ber. Bunsenges. Phys. Chem. 85 (1981) 693–704.
[4] M.R. Tarasevich, K.A. Radyushkina, Mater. Chem. Phys. 22 (1989) 477–502.
[5] S.L. Gupta, D. Tryk, I. Bae, W. Aldred, E.B. Yeager, J. Appl. Electrochem. 19 (1989) 19–27.
[6] A.L. Wijnoltz, Thesis, Eindhoven University of Technology, The Netherlands, 1995.
[7] G. Faubert, G. Lalande, R. Côté, D. Guay, J.P. Dodelet, L.T. Weng, Electrochim. Acta 41 (1996) 1689–1701.
[8] G. Lalande, G. Faubert, R. Côté, D. Guay, J.P. Dodelet, L.T. Weng, P. Bertrand, J. Power Sources 61 (1996) 227–237.
[9] S.Lj. Gojkovic, S. Gupta, R.F. Savinell, J. Electrochem. Soc. 145 (1998) 3493–3499.
[10] S.Lj. Gojkovic, S. Gupta, R.F. Savinell, J. Electroanal. Chem. 462 (1999) 63–72.
[11] R. Bashyam, P. Zelenay, Nature 443 (2006) 63–66.
[12] M. Lefevre, J.P. Dodelet, P. Bertrand, J. Phys. Chem. B 109 (2005) 16718–16724.
[13] F. Jaouen, J.P. Dodelet, J. Phys. Chem. C 111 (2007) 5963–5970.
[14] F. Charreteur, F. Jaouen, S. Ruggeri, J.P. Dodelet, Electrochim. Acta 53 (2008) 2925–2938.
[15] S. Maldonado, K.J. Stevenson, J. Phys. Chem. B 108 (2004) 11375–11383.
[16] S. Maldonado, K.J. Stevenson, J. Phys. Chem. B 109 (2005) 4707–4716.
[17] S. Maldonado, S. Morin, K.J. Stevenson, Carbon 44 (2006) 1429–1437.
[18] P.H. Matter, L. Zhang, U.S. Ozkan, J. Catal. 239 (2006) 83–96.
[19] P.H. Matter, E. Wanga, M. Ariasa, E.J. Biddinger, U.S. Ozkan, J. Mol. Catal. A 264 (2007) 73–81.
[20] P.H. Matter, E. Wang, J.-M.M. Millet, U.S. Ozkan, J. Phys. Chem. C 111 (2007) 1444–1450.
[21] N.P. Subramanian, X. Li, V. Nallathambi, S.P. Kumaraguru, H. Colon-Mercado, G. Wu, J.-W. Lee, B.N. Popov, J. Power Sources 188 (2009) 38–44.
[22] V. Nallathambi, J.-W. Lee, S.P. Kumaraguru, G. Wu, B.N. Popov, J. Power Sources 183 (2008) 34–42.
[23] E. Yeager, Electrochim. Acta 29 (1984) 1527–1537.
[24] K. Wiesener, Electrochim. Acta 31 (1986) 1073–1078.
[25] X.G. Li, W. Xing, T.H. Lu, Y.P. Ji, H.Y. Liang, Y. Shao, Chem. J. Chin. Univ. 24 (2003) 1246–1250.
[26] G.Q. Sun, J.T. Wang, R.F. Savinell, J. Appl. Electrochem. 28 (1998) 1087–1093.

[27] X.G. Li, W. Xing, Y.W. Tang, T.H. Lu, Chemistry (Huaxue Tongbao) 66 (2003) 521–527.
[28] M. Bron, S. Fiechter, P. Bogdanoff, H. Tributsch, Fuel Cells: Fundam. Syst. 2 (2002) 137–142.
[29] M. Lefèvre, J.P. Dodelet, Electrochim. Acta 48 (2003) 2749–2760.
[30] S.Lj. Gojković, S. Gupta, R.F. Savinell, Electrochim. Acta 45 (1999) 889–897.
[31] J. Willsau, J. Heitbaum, J. Electroanal. Chem 161 (1984) 93–101.
[32] Y. Shao, G. Yin, Y. Gao, J. Power Sources 171 (2007) 558–566.
[33] W.C. Schumb, C.N. Satterfield, R.L. Wentworth, Hydrogen Peroxide, Reinhold, New York, 1955.
[34] J.R. Anderson, Structure of Metallic Catalysts, Academic Press, London, 1975.
[35] B. O'Regan, M. Gratzel, Nature 353 (1991) 737–739.
[36] K. Liu, S. Shen, H. Xu, Acta Phys. Chim. Sin. 16 (2000) 1103–1109.
[37] R. Jiang, D. Chu, J. Electrochem. Soc 147 (2000) 4605–4609.
[38] O. Solorza-Feria, S. Ramírez-Raya, R. Rivera-Noriega, E. Ordoñez-Regil, S.M. Fernández-Valverde, Thin Solid Films 311 (1997) 164–170.
[39] U.A. Paulus, A. Wokaun, G.G. Scherer, T.J. Schmidt, V. Stamenkovic, V. Radmilovic, N.M. Markovic, P.N. Ross, J. Phys. Chem. B 106 (2002) 4181–4191.
[40] K. Suárez-Alcántara, O. Solorza-Feria, Electrochim. Acta 53 (2008) 4981–4989.
[41] X. Li, L. Liu, J.-W. Lee, B.N. Popov, J. Power Sources 182 (2008) 18–23.
[42] K. Kinoshita, J.A.S. Bett, Carbon 11 (1973) 403–411.
[43] H. Wang, R. Côté, G. Faubert, D. Guay, J.P. Dodelet, J. Phys. Chem. B 103 (1999) 2042–2049.
[44] B. Li, X. Wang, M. Yan, L. Li, Mater. Chem. Phys. 78 (2003) 184–188.
[45] S. Shanmugam, A. Gabashvili, D.S. Jacob, J.C. Yu, A. Gedanken, Chem. Mater. 18 (2006) 2275–2282.